Rapid Communications

Flat band quantum scar

Yoshihito Kuno, Tomonari Mizoguchi, and Yasuhiro Hatsugai
Department of Physics, University of Tsukuba, Tsukuba, Ibaraki 305-8571, Japan

(Received 12 October 2020; accepted 7 December 2020; published 23 December 2020)

We show that a quantum scar state, an atypical eigenstate breaking eigenstate thermalization hypothesis embedded in a many-body energy spectrum, can be constructed in flat band systems. The key idea of our construction is to make use of orthogonal compact localized states. We concretely discuss our construction scheme, taking a sawtooth flat lattice system as an example, and numerically demonstrate the presence of a quantum scar state. Examples of higher-dimensional systems are also addressed. Our construction method of quantum scar has broad applications to various flat band systems.

DOI: 10.1103/PhysRevB.102.241115

Introduction. Violation of eigenstate thermalization hypothesis (ETH) [1–4] now attracts great interest, being called weak ETH [5,6]. The violation leads to area-law entanglement entropy (EE) for some specific eigenstates, while almost all eigenstates exhibit thermalization and volume-law EE. Recently, a Rydberg cold-atom quantum simulator heuristically accessed specific eigenstates inducing the violation of the ETH through a quench dynamics [7]. A suitable nonentangled state (charge density wave state) has not thermalized during a long-time evolution and a recurrence occurs, indicating that the initial information is not lost. Immediately, the theoretical model describing the Rydberg cold-atom quantum simulator, namely, the PXP model, has been studied in detail and the study clarified that the series of nonthermalized eigenstates with the area-law EE exists, but the system is nonintegrable as a whole (there are no extensive numbers of the local conserved quantities) and a quench dynamics exhibits a coherence, corresponding to very-slow thermalization and linear (slow) growth of EE [8–13]. Such specific eigenstates not possessing the typical properties from the ETH are buried in most thermal eigenstates [14]. They are now called quantum scars (QSs), whose single-particle counterpart has been reported four decades ago [15].

QSs can appear not only for the PXP model but also for broad condensed-matter models. In fact, exact eigenstates with long-range orders away from the ground states were known in the literature, such as an η-pairing state in a Hubbard model [16,17], and indeed revisited as a candidate of QSs [18–20]. Recently, a general construction has been proposed [14] before the first Rydberg experiment [7]. Since then, an increasing number of examples have been reported, including the AKLT model [21,22], some $S = 1$ and $1/2$ spin models [23–26], topological models [27,28], frustrated spin systems [29], a quantum dimer model [30], and disordered systems [31,32]. Furthermore, a lattice supersymmetric lattice model [33] and two-dimensional Rydberg-atom system [34] has been theoretically expected to have QS states, and robust nonstationary dynamics related to QS has been reported [35,36].

In this Rapid Communication, we propose a simple general construction of QS states in flat band systems, where the model has a spatially compact localized state (CLS) [37–39] as eigenstates on the flat band, which does not spatially overlap, and thus are orthogonal with each other. This construction of the QS does not require implementation of complex and artificial interactions. They are standard nearest-neighbor density-density interactions. Therefore the scheme we are proposing can be applicable to various flat band systems. By making use of orthonormalized CLSs, we can construct a low entangled many-body state violating the ETH, which remains to be an exact eigenstate even in the presence of conventional density-density interaction; other states obey the ETH as the models themselves are generally nonintegrable. In the following, we first present a generic argument mentioned above, and then present a concrete example of the sawtooth-lattice model. We numerically demonstrate the realization of the QS state by showing the level statistics and time evolution of the entanglement. In addition, some examples of a two-dimensional model are presented.

General construction. We propose a general construction for a unique QS. We start with considering the following general flat band model with interactions for spinless fermions [40]. Let us consider a lattice with N_t sites composed of a periodic array of N_L unit cells; there are N_t/N_L sublattices per unit cell. On this lattice, we consider the Hamiltonian

$$H_{\rm tot} = H_0 + H_{\rm int}, \tag{1}$$

$$H_0 = \sum_{ij} f_i^\dagger h_{ij} f_j, \quad H_{\rm int} = \sum_{|i-j|\leqslant \ell} V_{ij} n_i n_j. \tag{2}$$

Here, H_0 stands for the single-particle Hamiltonian hosting a flat band with $f_i^{(\dagger)}$ being an annihilation (creation) fermion operator in real space, and $H_{\rm int}$ is a two-body finite-range interaction with the maximum range ℓ, V_{ij} is an interaction strength, and $n_j = f_j^\dagger f_j$. It is to be emphasized that elaborate turning of $H_{\rm int}$ is not needed to obtain the QS state. $H_{\rm int}$ is a natural short-range density-density interaction. Rather, the

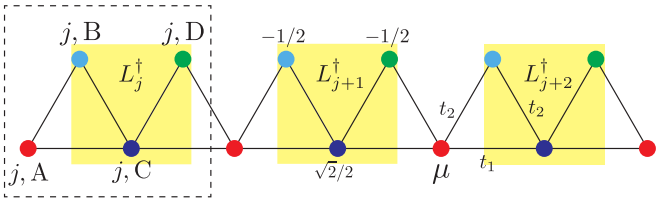

FIG. 1. Schematic picture of sawtooth lattice. The yellow shaded object is a CLS. The CLSs do not spatially overlap each other due to the presence of a finite μ. The minimum distance between the neighboring CLS is $d_m = 2$.

key feature to obtain the QS state is encoded in H_0, that is, we assume that the flat band eigenstates are spanned by *orthonormalized* localized states which have a compact support and do not spatially overlap each other; such states are referred to as the CLSs (see yellow shaded objects in Fig. 1 as an example). It is noteworthy that not all the flat band models satisfy this assumption. In fact, in some models, such a set of localized states either overlap each other or do not have a compact support [41,42].

Let L_j be an annihilation operator of the CLS at the unit cell $j \in [0, N_{\rm L} - 1]$, and d_m be the minimum of the distance between the sites involved in the support of neighboring L_j's, assumed to satisfy $d_m > 1$. Then, for the many-body system with particle number being fixed to $N_{\rm L}$, we consider the following state:

$$|\Psi_{\rm L}\rangle = \prod_{j=0}^{N_{\rm L}-1} L_j^\dagger |0\rangle. \tag{3}$$

This state is created by occupying all of the eigenstates on the flat band. Notably, for a finite-ranged $H_{\rm int}$, we can keep the state $|\Psi_{\rm L}\rangle$ an exact eigenstate due to the isolation of the CLS state [43]. Namely, if the interaction $H_{\rm int}$ is a two-body interaction under the condition $\ell < d_m$, the state $|\Psi_{\rm L}\rangle$ is still an eigenstate for the interacting system, because $H_{\rm int}|\Psi_{\rm L}\rangle = 0$, while $H_{\rm int}$ converts the total system into a nonintegrable system. In the literature, exact many-body eigenstates with vanishing interaction energy were considered in the context of flat band ferromagnetism [44–46], and later in the Wigner crystal [47]. As a result, $|\Psi_{\rm L}\rangle$ is a unique QS, which originates from the flat band nature, and we expect that $|\Psi_{\rm L}\rangle$ satisfies area-law scaling for the EE and is embedded in most thermal eigenstates in a system with a translational invariance. Further, the total system does not have extensive numbers of conserved quantities, so the total system is nonintegrable.

It should be noted that our construction has a relation to the recent general construction method by Shiraishi and Mori [14] (see Supplemental Material [48]). Our construction is also related to a toy model proposed in Eq. (7) in Ref. [10]. The first term of the toy model can be regarded as a trivial flat band, and the QS belongs to the kernel of the second operator, which also makes the toy model nonintegrable.

Example: Sawtooth lattice. By applying the above general argument, we show a concrete construction of the QS from CLSs, which is analytically very simple. We start with the following model defined on the sawtooth lattice (Fig. 1), $H_0 = \sum_{j=0}^{L-1}[t_1 f_{j,\rm A}^\dagger f_{j,\rm C} + t_2 f_{j,\rm A}^\dagger f_{j,\rm B} + t_2 f_{j,\rm B}^\dagger f_{j,\rm C} + t_1 f_{j,\rm C}^\dagger f_{j+1,\rm A} + t_2 f_{j,\rm C}^\dagger f_{j,\rm D} + t_2 f_{j,\rm D}^\dagger f_{j+1,\rm A} + {\rm H.c.}] + \sum_{j=0}^{L-1} \mu f_{j,\rm A}^\dagger f_{j,\rm A}$, and $H_{\rm int}$ is a nearest-neighbor interaction, given later [see Eq. (5)]. Note that the finite on-site potential, $\mu \neq 0$, leads to the increase of the sublattice degrees of freedom from two to four. Further, for $t_2 = \sqrt{2}t_1$, one band out of the four becomes a flat band (see Supplemental Material [48] for the single-particle spectrum). The existence of the flat band can be inferred from the molecular-orbital (MO) representation [48], which was developed to describe generic flat band models in the prior works [49,50]. We can also straightforwardly find *orthonormalized* CLSs as

$$L_j^\dagger = \tfrac{1}{2}[\sqrt{2} f_{j,\rm C}^\dagger - f_{j,\rm B}^\dagger - f_{j,\rm D}^\dagger], \quad \{L_j, L_{j'}^\dagger\} = \delta_{jj'}, \tag{4}$$

where L_j's do not overlap each other, and satisfy $[L_j^\dagger, H_0] = -2t_1 L_j^\dagger$. In some ferromagnetic spin models, similar CLSs were proposed but they are generically nonorthogonal [51,52].

Having these CLSs at hand, we now construct a many-body state, which turns into a QS when switching on interactions. We consider 1/4 filling, then can construct the many-body state that occupies all the states of the flat band, given in the form of Eq. (3). Clearly, this state is an exact eigenstate since $H_0|\Psi_{\rm L}\rangle = -2t_1 L|\Psi_{\rm L}\rangle$ and $H_{\rm int}|\Psi_{\rm L}\rangle = 0$. This fact is independent of the value of μ and the profile of V_{ij} ($|i - j| = 1$). Further, since $H_{\rm int}$ is a nearest-neighbor interaction and d_m for L_j's is equal to two, $|\Psi_{\rm L}\rangle$ is the eigenstate of $H_{\rm int}$ with zero eigenvalue, thus, $|\Psi_{\rm L}\rangle$ remains as a many-body eigenstate of $H_{\rm tot}$. The Wigner-solidlike particle distribution of $|\Psi_{\rm L}\rangle$ indicates that the state exhibits area-law EE. This state is atypical because the other many-body eigenstates are thermal delocalized, and are expected to obey the ETH and exhibit volume-law EE. In the following, we numerically demonstrate that $|\Psi_{\rm L}\rangle$ is the QS embedded in this model.

Numerical demonstration. Let us numerically verify that $|\Psi_{\rm L}\rangle$ is the QS state [53]. For concreteness, we set the profile of $H_{\rm int}$ as

$$H_{\rm int} = \sum_j V_0\left(n_j^{\rm A} n_j^{\rm B} - n_j^{\rm B} n_j^{\rm C} + n_j^{\rm C} n_j^{\rm D} - n_j^{\rm D} n_{j+1}^{\rm A}\right), \tag{5}$$

where $n_j^\alpha = f_{\alpha,j}^\dagger f_{\alpha,j}$ ($\alpha = {\rm A, B, C, D}$). Hereafter we set $t_1 = 1$.

As a first step, we demonstrate the nonintegrability from level spacing analysis. To be concrete, we calculate the level spacing r_s defined by $r_s = [\min(\delta^{(s)}, \delta^{(s+1)})]/[\max(\delta^{(s)}, \delta^{(s+1)})]$ for all s, where $\delta^{(s)} = E_{s+1} - E_s$ and $\{E_s\}$ is the set of energy eigenvalue (in ascending order), and calculate the mean level spacing $\langle r\rangle$ which is obtained by averaging over r_s by employing all energy eigenvalues with fixed momentum space. By introducing a parameter α as $\mu = -2\alpha$ and $V_0 = 3\alpha$, we observe nonintegrable behaviors of the system. Figure 2(a) is the numerical result. As increasing α, $\langle r\rangle$ shows a clear crossover from integrable ($\langle r\rangle \simeq 0.39$, corresponding to the Poisson distribution) to nonintegrable ($\langle r\rangle \simeq 0.53$, corresponding to the Wigner-Dyson distribution). Hence, the term $H_{\rm int}$ makes the system nonintegrable. In what follows, we focus on the nonintegrable parameter point $\alpha = 1$.

To verify the presence of the QS state $|\Psi_{\rm L}\rangle$, we next calculate an overlap $|\langle Z_4|\Psi_\ell\rangle|$, where $|Z_4\rangle = \prod_{j=0} f_{C,j}^\dagger |0\rangle$ and $|\Psi_\ell\rangle$ is a many-body eigenstate for $H_{\rm tot}$. As a typical character,

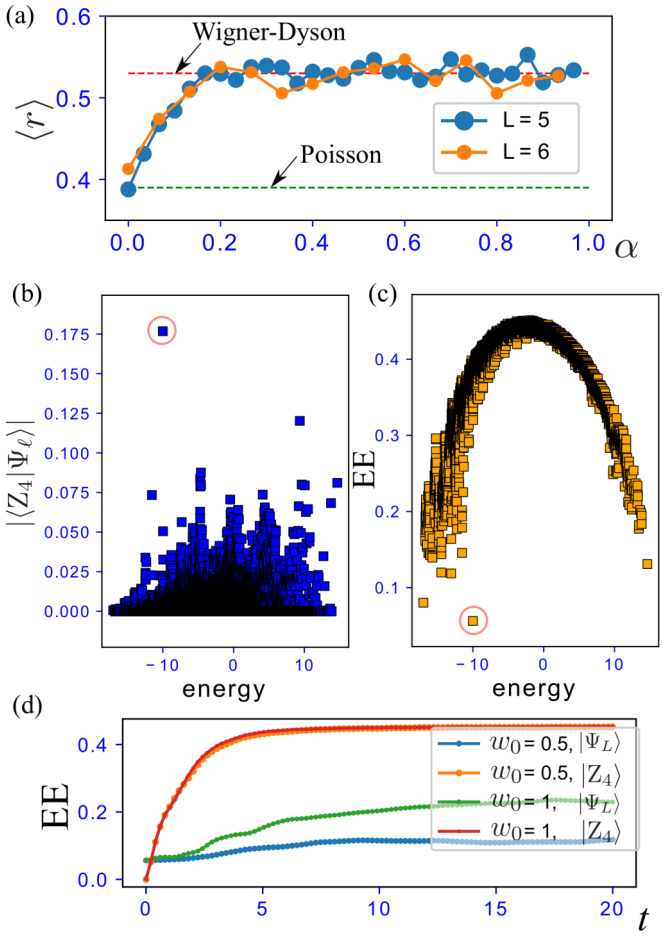

FIG. 2. Numerical results for the sawtooth lattice model. (a) Mean level spacing $\langle r\rangle$ averaged over all energy eigenvalues in the momentum sector $k = 0$ (see [8,55]). We set $L = 5$ with five particles and $L = 6$ with six particles. (b) Overlap to $|Z_4\rangle$ for all eigenstates. The red circle indicates $|\Psi_L\rangle$. (c) Distribution of EE. The EE is normalized by the number of sites in the subsystem. The red circle indicates $|\Psi_L\rangle$. The EE for the red circle is very small because the only single CLS is cut; the value is $s_{\min} = \frac{1}{2L}(2\ln 2 - \frac{3}{4}\ln 3) \approx 0.056\,23$. For (b) and (c), we set $\mu = -2$, $V_0 = 3$, and $L = 5$ with five particles. (d) Single-shot quench dynamics of EE: the disorder is $\mu_{A,j}, \mu_{B,j} \in [-w_0, w_0]$ with $V_0 = 3$. We set $L = 5$ with five particles and two initial states, $|\Psi_L\rangle$ and $|Z_4\rangle$.

we expect that $|\Psi_L\rangle$ has large overlap compared to the other eigenstates. The result is shown in Fig. 2(b). We find an atypical state with a large overlap, which is nothing but $|\Psi_L\rangle$.

Next, we divide the system into two parts where both parts include $2L$ lattice sites and calculate the EEs of all eigenstates for the subsystem [54]. The result is shown in Fig. 2(c). We find that the QS state $|\Psi_L\rangle$ embedded in the energy excitation band exhibits very low-valued EE while other eigenstates have large value of the EE and show an arched distribution, which is a typical character of thermalized states in various systems [27,28,30]. Actually, the value of the EE for $|\Psi_L\rangle$ can be easily obtained from cutting the single CLS. The simple calculation is shown in the Supplemental Material [48]. The numerical result of the EE for the QS agrees with the analytical result.

Additionally, we investigate the effects of static disorders for the system. Through observing EE in the quench dynamics of the system, we investigate the following: (i) How robust is the QS for clean system $|\Psi_L\rangle$ to disorders? (ii) Whether or not a weakly disordered system has a similar QS state in the clean limit. In dynamics, we set two initial states $|\Psi_L\rangle$ and $|Z_4\rangle$ and calculate the unitary dynamics by using exact diagonalization. Here we introduce a random on-site potential, i.e., adding the following term: $H_{\text{rand}} = \sum_{j,\alpha} \mu_j^\alpha n_j^\alpha$ with $\mu_j^\alpha \in [-w_0, w_0]$. We fix $\mu = 0$ and $V_0 = 3$. In the presence of H_{rand}, $|\Psi_L\rangle$ is no longer an exact eigenstate. The result is presented in Fig. 2(d), where we see the EE of the initial $|Z_4\rangle$ suddenly increases and reaches a saturation value. On the other hand, the growth of EE for the initial $|\Psi_L\rangle$ is very slow. This implies that for the disordered system, there exists a QS which is very close to $|\Psi_L\rangle$. We also investigate another type of disorder that keeps $|\Psi_L\rangle$ an exact eigenstate (see the Supplemental Material [48]).

Extension to higher dimensions. The construction of the QS is applicable in higher dimensions. Here we present three concrete examples in two dimensions.

The first example is the real hopping model on a kagome lattice [Fig. 3(a)]. Here we set the nearest-neighbor hopping t, being real, and the on-site potentials are set as μ_1 for red dots, μ_2 for blue dots, μ_3 for green dots, and 0 otherwise. Due to the modulation of the on-site potential, the unit cell is enlarged compared with the conventional kagome model, resulting in nine sublattice degrees of freedom. In this model, the CLSs reside on hexagons denoted by yellow shades in Fig. 3(a), whose wave function has a staggered sign structure [42,56–58]. Clearly, d_m is equal to two, and thus the CLSs do not overlap each other. This is a sharp contrast to the kagome model without on-site potentials, where CLSs live on all the hexagons and thus they overlap each other. The band structure is depicted in Fig. 3(b). We see an isolated flat band at $E = -2t$. Thus, when including the nearest-neighbor interaction and considering the 1/9-filled system, we obtained the QS in the form of Eq. (3).

The second example is the pure imaginary hopping model on a kagome lattice [Fig. 3(c)]. The model without the on-site potential is investigated in the context of topological phase [59,60]. In fact, the CLSs again reside on the hexagons but the wave function has a uniform sign structure. Then, we again find a flat band, as shown in Fig. 3(d). Moreover, the dispersive bands possess finite Chern number, which may lead to additional intriguing physics due to topology. Due to the CLSs, we can again construct the scar state at 1/9-filling. Note that the flat band touches the dispersive band at the Γ point, resulting in additional degeneracy for the noninteracting case. Nevertheless, this additional degeneracy will be lifted when introducing the interaction, as the additional state is extended thus the many-body states occupying this state cost interaction energy.

The third example is the square kagome model [Fig. 3(e)]. The model has two hopping parameters, t_1 and t_2. Remarkably, in this model, the CLSs with $d_m = 2$ appear without incorporating the on-site potential. To be concrete, the CLSs are on the square plaquettes, and have a staggered sign structure [61]. The band structure is shown in Fig. 3(f). We find a flat band corresponding to the CLSs, indicating the existence of

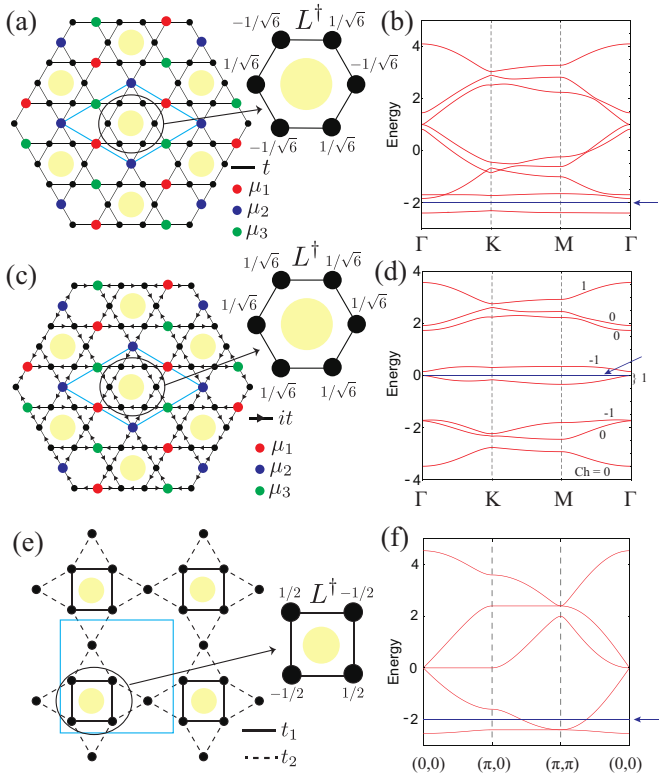

FIG. 3. (a) Schematic figure of the kagome model with real hoppings. The CLSs are located at the hexagons on which the yellow shaded balls are placed. (b) The band structure for $(t, \mu_1, \mu_2, \mu_3) = (1, 0.5, 0.75, -0.8)$. The high-symmetry points in the Brillouin zone are $\Gamma = (0, 0)$, $K = (\frac{2\pi}{\sqrt{3}a_0}, \frac{2\pi}{3a_0})$, and $M = (\frac{\pi}{\sqrt{3}a_0}, \frac{\pi}{a_0})$, with a_0 being the lattice constant. The blue line represents the flat band. (c) Schematic figure of the kagome model with pure imaginary hoppings. The CLSs are located at the hexagons on which the yellow shaded balls are placed. (d) The band structure for $(t, \mu_1, \mu_2, \mu_3) = (1, 0.5, 0.75, -0.8)$. The blue line represents the flat band. The Chern number is shown beside each band. (e) Schematic figure of the square kagome model. The CLSs are located at the square plaquettes on which the yellow shaded balls are placed. (f) The band structure for $(t_1, t_2) = (1, 1.2)$. The blue line represents the flat band.

the QS at 1/6-filling. Again, the flat band is degenerated with the dispersive band but it does not affect the emergence of the QS. It would also be interesting to remark that the QS is found in the localized spin model on the square kagome lattice as well [29].

Multiple QS. Although we have discussed a unique QS, one can also construct multiple QSs by reducing the number of CLSs in Eq. (3), and also the sawtooth lattice and the kagome lattice *without* on-site potentials.

We further remark that our construction is extensible to systems with multiple flat bands (i.e., with different types of CLS), if we can fill CLSs spatially separated from each other. In such a case, possible patterns of filling CLSs become abundant, which results in multiple QSs. Candidates for such systems include metal organic frameworks (MOFs) [62–64] and covalent organic frameworks (COFs) [65–67], where the tuning of electron filling may be feasible by using gate tuning or chemical doping.

Conclusion. We propose a general construction scheme of flat band QSs, making use of the orthonormalized CLSs. As a simple example, we numerically demonstrate the presence of the unique QS for a sawtooth lattice model, which can be implemented in cold-atom optical lattice systems [68,69]. We also present some examples of higher dimensions, namely, kagome and square kagome lattice systems. We expect that our construction of the unique QS for nonoverlapping CLSs has very wide-range applications for a Wigner-crystal state on a p_{x-y}-orbital honeycomb lattice system [47], and not only for fermions but also for hard-core bosons, which is related to the recent experiments on Rydberg atoms [70]. In our construction of the QS, elaborate tuning of interactions is not needed to obtain the QS state, and a natural form of interactions is allowed. This is the advantage for experimental implementation.

Further, as we have mentioned above, searching QSs in chemical systems such as MOFs and COFs will be another interesting direction. Thus, our work will open up a way for realizing QSs in a broader class of systems. Needless to say, based on flat band models, the construction of multiple scar states and finding athermal revival dynamics are interesting future problems.

Acknowledgments. We thank H. Katsura and T. Mori for valuable comments and discussion. This work is supported in part by JSPS KAKENHI Grants No. JP17H06138 (Y.K., T.M., Y.H.) and No. JP20K14371 (T.M.).

[1] J. M. Deutsch, Phys. Rev. A **43**, 2046 (1991).
[2] M. Srednicki, Phys. Rev. E **50**, 888 (1994).
[3] M. Rigol, V. Dunjko, V. Yurovsky, and M. Olshanii, Phys. Rev. Lett. **98**, 050405 (2007).
[4] M. Rigol, V. Dunjko, and M. Olshanii, Nature (London) **452**, 854 (2008).
[5] L. D' Alessio, Y. Kafri, A. Polkovnikov, and M. Rigol, Adv. Phys. **65**, 239 (2016).
[6] C. Gogolin and J. Eisert, Rep. Prog. Phys. **79**, 056001 (2016).
[7] H. Bernien, S. Schwartz, A. Keesling, H. Levine, A. Omran, H. Pichler, S. Choi, A. S. Zibrov, M. Endres, M. Greiner *et al.*, Nature (London) **551**, 579 (2017).
[8] C. J. Turner, A. A. Michailidis, D. A. Abanin, M. Serbyn, and Z. Papić, Nat. Phys. **14**, 745 (2018).
[9] C. J. Turner, A. A. Michailidis, D. A. Abanin, M. Serbyn, and Z. Papić, Phys. Rev. B **98**, 155134 (2018).
[10] S. Choi, C. J. Turner, H. Pichler, W. W. Ho, A. A. Michailidis, Z. Papić, M. Serbyn, M. D. Lukin, and D. A. Abanin, Phys. Rev. Lett. **122**, 220603 (2019).
[11] W. W. Ho, S. Choi, H. Pichler, and M. D. Lukin, Phys. Rev. Lett. **122**, 040603 (2019).
[12] C. J. Lin and O. I. Motrunich, Phys. Rev. Lett. **122**, 173401 (2019).
[13] V. Khemani, C. R. Laumann, and A. Chandran, Phys. Rev. B **99**, 161101(R) (2019).

[14] N. Shiraishi and T. Mori, Phys. Rev. Lett. **119**, 030601 (2017).
[15] E. J. Heller, Phys. Rev. Lett. **53**, 1515 (1984).
[16] C. N. Yang, Phys. Rev. Lett. **63**, 2144 (1989).
[17] S.-C. Zhang, Phys. Rev. Lett. **65**, 120 (1990).
[18] O. Vafek, N. Regnault, and B. A. Bernevig, SciPost. Phys. **3**, 043 (2017).
[19] D. K. Mark and O. I. Motrunich, Phys. Rev. B **102**, 075132 (2020).
[20] S. Moudgalya, N. Regnault, and B. A. Bernevig, Phys. Rev. B **102**, 085140 (2020).
[21] S. Moudgalya, N. Regnault, and B. A. Bernevig, Phys. Rev. B **98**, 235156 (2018).
[22] S. Moudgalya, S. Rachel, B. A. Bernevig, and N. Regnault, Phys. Rev. B **98**, 235155 (2018).
[23] M. Schecter and T. Iadecola, Phys. Rev. Lett. **123**, 147201 (2019).
[24] S. Chattopadhyay, H. Pichler, M. D. Lukin, and W. W. Ho, Phys. Rev. B **101**, 174308 (2020).
[25] K. Lee, R. Melendrez, A. Pal, and H. J. Changlani, Phys. Rev. B **101**, 241111(R) (2020).
[26] B. van Voorden, J. Minář, and K. Schoutens, Phys. Rev. B **101**, 220305(R) (2020).
[27] S. Ok, K. Choo, C. Mudry, C. Castelnovo, C. Chamon, and T. Neupert, Phys. Rev. Research **1**, 33144 (2019).
[28] N. S. Srivatsa, J. Wildeboer, A. Seidel, and A. E. B. Nielsen, Phys. Rev. B **102**, 235106 (2020).
[29] P. A. McClarty, M. Haque, A. Sen, and J. Richter, Phys. Rev. B **102**, 224303 (2020).
[30] J. Wildeboer, A. Seidel, N. S. Srivatsa, A. E. B. Nielsen, and O. Erten, arXiv:2009.00022.
[31] O. Hart, G. De Tomasi, and C. Castelnovo, Phys. Rev. Research **2**, 043267 (2020).
[32] N. Shibata, N. Yoshioka, and H. Katsura, Phys. Rev. Lett. **124**, 180604 (2020).
[33] F. M. Surace, G. Giudici, and M. Dalmonte, Quantum **4**, 339 (2020).
[34] A. A. Michailidis, C. J. Turner, Z. Papi, D. A. Abanin, and M. Serbyn, Phys. Rev. Research **2**, 022065(R) (2020).
[35] B. Buča, A. Purkayastha, G. Guarnieri, M. T. Mitchison, D. Jaksch, and J. Goold, arXiv:2008.11166.
[36] M. Medenjak, B. Buča, and D. Jaksch, Phys. Rev. B **102**, 041117(R) (2020).
[37] D. Leykam, A. Andreanov, and S. Flach, Adv. Phys. X **3**, 1473052 (2018).
[38] F. D. R. Santos and R. G. Dias, Sci. Rep. **10**, 4532 (2020).
[39] P. Sathe, F. Harper, and R. Roy, arXiv:2008.05528.
[40] Here, this model is for any spatial dimension and lattice structure.
[41] D. L. Bergman, C. Wu, and L. Balents, Phys. Rev. B **78**, 125104 (2008).
[42] S. D. Huber and E. Altman, Phys. Rev. B **82**, 184502 (2010).
[43] Our construction of $|\Psi_L\rangle$ has similar characteristics to that of Ref. [31].In our construction, the essential point is to keep spatial distance, which avoids interaction effects. In Ref. [31], an adjacent arrangement of the CLSs was considered; the amplitude of the CLS is vanishing.
[44] A. Mielke, J. Phys. A: Math. Gen. **24**, L73 (1991); **24**, 3311 (1991).
[45] H. Tasaki, Phys. Rev. Lett. **69**, 1608 (1992).
[46] H. Tasaki, Prog. Theor. Phys. **99**, 489 (1998).
[47] C. Wu, D. Bergman, L. Balents, and S. Das Sarma, Phys. Rev. Lett. **99**, 070401 (2007).
[48] See Supplemental Material at http://link.aps.org/supplemental/10.1103/PhysRevB.102.241115 for (i) Comparison with Shiraishi-Mori construction, (ii) Single particle spectrum for saw-tooth lattice, (iii) Molecular orbital picture for saw-tooth lattice, (iv) Entanglement entropy for a single CLS in saw-tooth lattice and (v) Disorder effect to dynamics of entanglement entropy.
[49] Y. Hatsugai and I. Maruyama, Europhys. Lett. **95**, 20003 (2011).
[50] T. Mizoguchi and Y. Hatsugai, Europhys. Lett. **127**, 47001 (2019).
[51] J. Schulenburg, A. Honecker, J. Schnack, J. Richter, and H. J. Schmidt, Phys. Rev. Lett. **88**, 167207 (2002).
[52] O. Derzhko, J. Schnack, D. V. Dmitriev, V. Y. Krivnov, and J. Richter, Eur. Phys. J. B **93**, 161 (2020).
[53] For all numerical simulations, we employed the Quspin solver: P. Weinberg and M. Bukov, SciPost Phys. **7**, 20 (2019); **2**, 003 (2017).
[54] For example, if we set $L = 5$ system, the subsystem includes the lattice site, $(j, \alpha) = \{(0, A), (0, B), (0, C), (0, D), \ldots, [(L-1)/2, A], [(L-1)/2, B]\}$.
[55] L. F. Santos and M. Rigol, Phys. Rev. E **81**, 036206 (2010).
[56] M. E. Zhitomirsky and H. Tsunetsugu, Phys. Rev. B **70**, 100403(R) (2004).
[57] T. Bilitewski and R. Moessner, Phys. Rev. B **98**, 235109 (2018).
[58] J.-W. Rhim and B.-J. Yang, Phys. Rev. B **99**, 045107 (2019).
[59] K. Ohgushi, S. Murakami, and N. Nagaosa, Phys. Rev. B **62**, R6065(R) (2000).
[60] D. V. Else, H. C. Po, and H. Watanabe, Phys. Rev. B **99**, 125122 (2019).
[61] O. Derzhko and J. Richter, Eur. Phys. J. B **52**, 23 (2006).
[62] T. Kambe, R. Sakamoto, T. Kusamoto, T. Pal, N. Fukui, K. Hoshiko, T. Shimojima, Z. Wang, T. Hirahara, K. Ishizaka, S. Hasegawa, F. Liu, and H. Nishihara, J. Am. Chem. Soc. **136**, 14357 (2014).
[63] M. G. Yamada, T. Soejima, N. Tsuji, D. Hirai, M. Dincă, and H. Aoki, Phys. Rev. B **94**, 081102(R) (2016).
[64] A. Kumar, K. Banerjee, A. S. Foster, and P. Liljeroth, Nano Lett. **18**, 5596 (2018).
[65] Y. Shuku, A. Mizuno, R. Ushiroguchi, C. S. Hyun, Y. J. Ryu, B.-K. An, J. E. Kwon, S. Y. Park, M. Tsuchiizu, and K. Awaga, Chem. Commun. **54**, 3815 (2018).
[66] Y. Fujii, M. Maruyama, and S. Okada, Jpn. J. Appl. Phys. **57**, 125203 (2018).
[67] T. Mizoguchi, M. Maruyama, S. Okada, and Y. Hatsugai, Phys. Rev. Mater. **3**, 114201 (2019).
[68] T. Zhang and G.-B. Jo, Sci. Rep. **5**, 16044 (2015).
[69] P. Wang, L. Chen, C. Mi, Z. Meng, L. Huang, K. S. Nawaz, H. Cai, D.-W. Wang, S.-Y. Zhu, and J. Zhang, npj Quantum Inf. **6**, 18 (2020).
[70] S. De Léséleuc, V. Lienhard, P. Scholl, D. Barredo, S. Weber, N. Lang, H. P. Büchler, T. Lahaye, and A. Browaeys, Science **365**, 775 (2019).